Icarus 433 (2025) 116521

Contents lists available at ScienceDirect

Icarus

journal homepage: www.elsevier.com/locate/icarus

Fast firing technique for Martian regolith simulant: Advancing ISRU capabilities

Levent Karacasulu [a,b,*], Alessandro Tomasini [b], Cekdar Vakifahmetoglu [a], Mattia Biesuz [b]

[a] Department of Materials Science and Engineering, İzmir Institute of Technology, 35430 İzmir, Türkiye
[b] Department of Industrial Engineering, University of Trento, Via Sommarive 9, 38123 Trento, Italy

ARTICLE INFO

Keywords:
Fast firing
Sintering
Martian regolith simulant
MGS-1
ISRU

ABSTRACT

In-Situ Resource Utilization (ISRU) approaches hold significant importance in plans for space colonization. This work explores a different ISRU concept applying fast-firing, a robust and well-known industrial process, to Mars regolith simulant (MGS-1). The fast-fired specimens were compared to the ones obtained by conventional sintered under low heating rates. When the holding time at the firing temperature is longer than 15 min, fast-fired specimens exhibited higher density and flexural strength (> 35 MPa) than conventional sintering. For both processes, the bulk density values and the mechanical properties of the regolith compacts were enhanced with increasing dwell time. This was attributed to higher heating rates changing the densification/crystallization kinetics involving the basalt glass in the regolith composition. Specifically, high heating rate promotes sintering over crystallization. On these bases, fast firing can be considered a potential candidate for ISRU on Mars.

1. Introduction

Promising plans to colonize space require appropriate use of the available resources for a sustainable life outside our planet. In this sense, materials found in outer space deserve particular attention (Alexiadis et al., 2017). In-situ resource utilization (ISRU) is the on-site collection, processing, storing, and use of indigenous materials encountered during human or robotic space exploration. Therefore, early colonization scenarios propose using regoliths composed of various oxide minerals (Karl et al., 2018).

In previous studies, a few number of ISRU approaches of regolith simulants have been proposed, including dry consolidation (Chow et al., 2017; Meek et al., 1987; Simonds, 1973), melting (Blacic, 1985; Dalton and Hohmann, 1972; Zocca et al., 2020), geopolymerization (Alexiadis et al., 2017; Mills et al., 2022; Montes et al., 2015), self-propagating high-temperature synthesis (Corrias et al., 2012), slip casting (Karl et al., 2018), additive manufacturing (Altun et al., 2021; Karl et al., 2020a, 2020b), and cold sintering (Karacasulu et al., 2023). Clearly, further studies are still required to establish new ISRU approaches.

Generally, the regoliths obtained from Lunar or Mars contain largely silica (~50 wt%); this means it may be possible to produce glass or ceramics by sintering or melting (Hintze and Stephanie, 2013; Moses and Bushnell, 2016; Naser, 2019; Roberts et al., 2021; Rousek et al., 2012). Therefore, different sintering approaches, including conventional sintering under various atmospheric conditions (Dou et al., 2019; Han et al., 2022; Meurisse et al., 2017; Song et al., 2019; Warren et al., 2022), laser processing (Farries et al., 2022; Fateri and Gebhardt, 2015; Ginés-Palomares et al., 2023; Krishna Balla et al., 2012), solar sintering (Meurisse et al., 2018), cold sintering (Karacasulu et al., 2023), microwave sintering (Kim et al., 2021; Lim et al., 2021; Meek et al., 1987; Rousek et al., 2012; Taylor and Meek, 2005), spark plasma sintering (Licheri et al., 2022) have been proposed to densify such regoliths.

Fast firing (FF), introduced at the beginning of the 80s, is a fundamental "unconventional" sintering process. It allows rapid densification by utilizing a high heating rate (10^2–10^3 °C/min) with a short dwell time at the sintering temperature (Bordia et al., 2017; Harmer and Brook, 1981; Karacasulu et al., 2024). During FF, the green sample is introduced quickly into the hot zone of a pre-heated furnace to reach high temperatures in a few seconds/minutes. When considering crystalline ceramics, the fast-heating rate is crucial in enhancing densification by suppressing grain growth, thus facilitating consolidation (Bordia et al., 2017). For the same density, fast-fired samples generally result in smaller grain and pore size, and reduced pore/grain boundary separation (i.e., breakaway phenomenon) compared to the conventional sintering process (Bordia et al., 2017; Kim and Kim, 1993). This phenomenon is associated with the different activation energies for the

* Corresponding author at: Department of Industrial Engineering, University of Trento, Via Sommarive 9, 38123 Trento, Italy.
E-mail addresses: levent.karacasulu@unitn.it, leventkaracasulu@iyte.edu.tr, leventkaracasulu@gmail.com (L. Karacasulu).

https://doi.org/10.1016/j.icarus.2025.116521
Received 24 September 2024; Received in revised form 31 January 2025; Accepted 17 February 2025
Available online 18 February 2025

two processes, where densification (involving only bulk/grain boundary diffusion) is typically characterized by higher activation energy than coarsening and, as such, requires a higher temperature to be activated (Harmer and Brook, 1981; Kang, 2020; Leriche et al., 2017). However, the said considerations are valid only for crystalline systems where densification takes place via solid-state diffusion. More limited attention has been focused on the FF of systems characterized by liquid phase sintering or viscous flow sintering to which Mars regolith simulants belong.

Due to its rapidness and simplicity, fast-firing has gained popularity as a sintering technique with several industrial applications and has been used to sinter both traditional and advanced ceramics (Hotza et al., 2015). It could also be applied to an extra-terrestrial environment as it requires a heating element, a single chamber, and an electric power source, which could be integrated with a photovoltaic energy source.

The main goal of this work was to demonstrate proof of concept to sinter Mars regolith (MGS-1) simulant monoliths via fast firing technique for the first time. The densification ability of Martian regolith by FF was investigated, and the results were compared to those of conventional sintering.

2. Materials and methods

Various Martian Regolith simulants were developed (Allen et al., 1998a, 1998b; Cannon et al., 2019; Clark et al., 2020; Gupta et al., 2024; Karl et al., 2022) following the Mars Science Laboratory (MSL) rover Curiosity's X-ray diffraction (XRD) results of global basaltic soil at the Gale crater on Mars (Bish et al., 2013). Commercial and relatively economic (~50 $ / kg current price, 2024 current price) sources are also available, e.g., a selected MGS-1 simulant was acquired from Space Resource Technologies (SRT, USA). The simulant bulk chemistry is constituted by approximately 45 wt% SiO_2, with the remainder composed mainly of Al_2O_3, FeO, MgO, CaO, and Na_2O with ~5 wt% loss on ignition (LOI), measured by X-ray fluorescence (XRF) (Long-Fox and Britt, 2023). Although mineralogic compositions of regolith simulants vary from batch to batch, the MGS-1 has plagioclase (27.1 %), glass-rich basalt (22.9 %), pyroxene (20.3 %), olivine (13.7 %), Mg-sulfate (4 %), ferrihydrite (3.5 %), hydrated silica (3.5 %), magnetite (1.9 %), anhydrite (1.7 %), Fe-carbonate (1.4 %), and hematite (0.5 %), all in wt%. It should be underlined that the powder characteristics, such as raw material sources, size distribution, and angle of repose, can also alter (Long-Fox and Britt, 2023).

MGS-1 simulant powder was initially milled by vibratory milling and sieved in a 60-mesh sieve to reduce the particle size. Measurement of the particle size distribution of the as-received and milled powders was performed utilizing the dry measurement with an assumption of a refractive index of 1.5 (Martikainen et al., 2023) by a laser scattering particle size analyzer (Partica LA-960 V2, Horiba, Japan). Thermogravimetric analysis (TGA) of the MGS-1 powder was conducted in an air atmosphere up to 1200 °C with a heating rate of 20 °C/min using the thermobalance STA 409 (NETZSCH Geraetebau GmbH, Germany). True density was measured with 99 repetitions using a helium gas pycnometer Ultrapyc 5000 (Anton Paar GmbH, Graz, Austria), with integrated Peltier cell temperature control of the measuring chamber.

0.2 g of MGS-1 simulant was uniaxially pressed in a cylindrical die with an 8 mm diameter under a pressure of 200 MPa. To understand the sintering characteristics of the MGS-1 simulant, the optical dilatometry analysis was performed on the pressed MGS-1 green bodies at a heating rate of 2.5–50 °C/min using a heating microscope (EM301, Hesse Instruments, Osterode am Harz, Germany). The green samples were sintered by fast firing and conventional sintering. For the fast firing process, the obtained pellets were inserted quickly into the hot zone of the tube furnace (Nabertherm P330, Lilienthal, Germany) at the selected temperatures (1080–1120-1160 °C) and kept there for varying times ranging from 1 min to 1 h. After the set dwell time, the samples were rapidly taken out from the furnace. The conventional sintering experiments were carried out in the same furnace under 5 °C/min heating and cooling rate. The sintering temperature and dwelling time were the same as for FF.

The bulk densities of the samples were determined by Archimedes' method using water as a buoyancy medium and a balance with a sensitivity of 0.1 mg. The polished surfaces were observed by scanning electron microscopy (SEM) (JEOL Ltd.©, JSM-5500, Tokyo, Japan). Phase analysis was conducted by X-ray diffractometer (XRD, Ital-structures IPD3000 diffractometer, Italy) with a copper anode X-ray source (CuK_α = 1.5406 Å). Scans were carried out in between the 10°–130° (2θ) range with 0.2°/s. To determine mechanical properties, the flexural strength values of the produced specimens were calculated using the piston-on-three balls test (Shetty et al., 1980). The piston-on-three balls test was performed using an MTS 810 mechanical testing machine equipped with a 5-kN load cell at a loading rate of 0.1 mm/s.

3. Results and discussion

Fig. 1**(a,b)** shows particle characteristics of MGS-1 regolith simulants used for conventional sintering and fast-firing. The particle size distribution (PSD) data for the milled MGS-1 powder revealed a multimodal distribution, as given in Fig. 1(a). After milling, the median particle size (d_{50}) was around 14 μm. The true density of the used MGS-1 simulant powder was found to be 2.89 g/cm^3 by using a gas pycnometer.

Fig. 1(b) reports the TGA/DTA analysis of MGS-1 simulant powder. TGA analysis demonstrated about ~4.7 % total weight loss until 1200 °C for the MGS-1 simulant, which is consistent with the result (~4 %) at 1000 °C by Cannon et al. (Cannon et al., 2019) and the LOI of 5 wt % as reported by Long-Fox and Britt (Long-Fox and Britt, 2023). Typically, the main losses in the TGA analysis are accompanied by firstly the loss of physisorbed water around 100 °C and then chemisorbed water until around 400 °C, and then the decomposition of carbonates and sulfates in the regolith composition (mainly Fe-carbonate and Mg-sulfate, and anhydrite). It should be noted that the MGS-1 simulant contains a considerable amount of iron constituents (e.g., Fe-carbonate) susceptible to oxidation in the air environment, which might slightly affect weight loss (Kądziołka-Gaweł et al., 2023).

Fig. 2(a) reports shrinkage of the MGS-1 regolith compact upon heating with 2.5, 5, 10, 25, and 50 °C/min up to 1200 °C. We observe that up to 1080 °C the sample undergoes thermal expansion when low heating rates are considered. Surprisingly, no noticeable difference in sintering shrinkage/temperature plot was observed under "low" heating rates, especially for 2.5, 5, and 10 °C/min. When considering higher heating rates (25 and 50 °C/min), the shrinkage occurs at a lower temperature and increases in magnitude. Besides, some similarities might be spotted with previous works on JSC-2A Lunar regolith (Zocca et al., 2020), usually, increasing the heating rate, the opposite behavior in ceramics is expected: when heating is fast, the sintering curves shift to the right, i.e., at higher temperatures, as a result of the reduction in the time available for mass transport to occur. Our results highlight that increasing the heating rate sintering is facilitated. The impact of the heating rate is relevant, considering that comparing the different samples, the time available for densification varies by a factor of 20×.

Fig. 2(b) shows hot-stage microscopy images of the sintered simulants at 700–1200 °C. While no observable shrinkage could be found even at 1100 °C in the samples produced under low heating rates, shrinkage has already started in the high-speed samples. The difference between the shrinkages at the determined sintering temperature (1160 °C) is also clearly visible. Higher temperatures make the materials melt and lose shape (1200 °C). Note that the area increase above 1160–1180 °C (Fig. 2(a)) is not really due to a swelling of the material but likely originates just from the loss in the sample geometry.

Besides, the glass transition temperature (T_g) of glass-basalt in the regolith composition was detectable by dilatometry. Its signature is the slope change at around 910 °C in the thermal expansion plots visible in

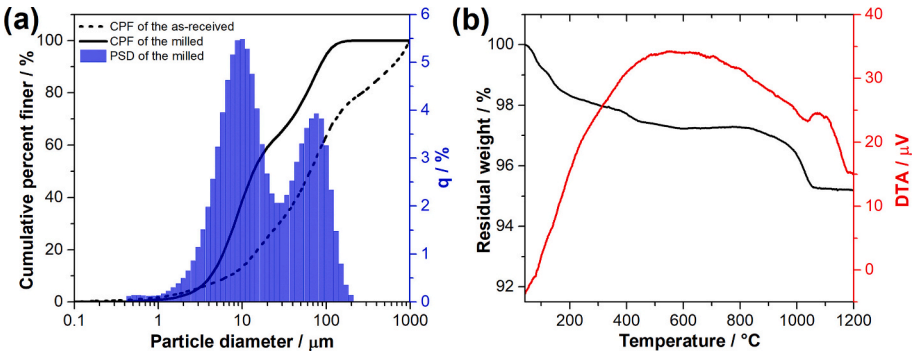

Fig. 1. Characteristics of MGS-1 regolith simulant, (a) particle size distribution (PSD) data of the milled MGS-1 regolith powders with cumulative percent finer (CPF) data of the as-received and the milled, and (b) TG / DTA analysis of MGS-1 simulant.

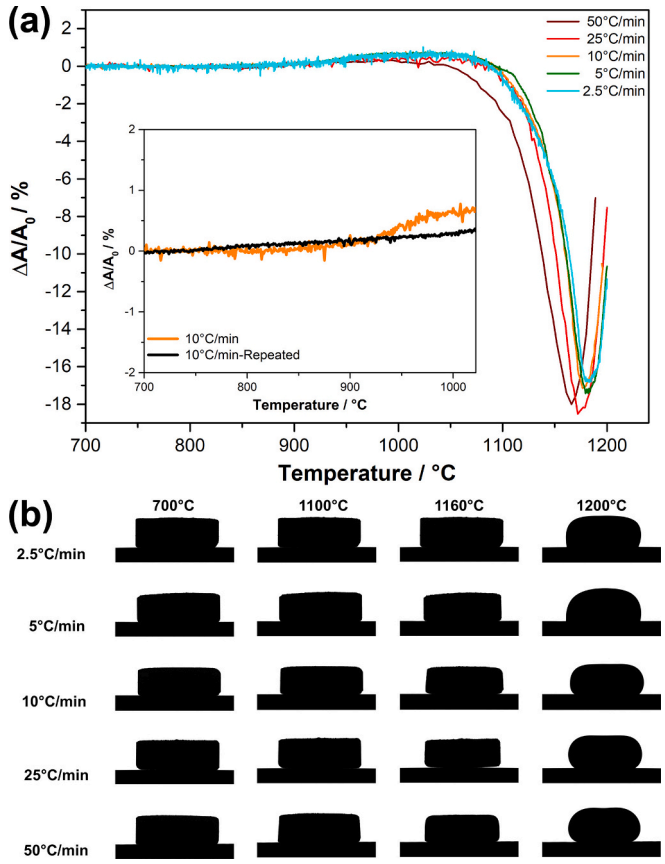

Fig. 2. (a) Dilatometer curves of green MGS-1 pellet with different heating rates and the bottom-left inset shows the determination of glass transition temperature (T_g) by dilatometry, **(b)** Hot stage microscopy images of MGS-1 pellets at different temperatures. (For interpretation of the references to colour in this figure legend, the reader is referred to the web version of this article.)

the inset of Fig. 2(a). After heating a sample up to 1200 °C (10 °C/min) in the optical dilatometer, it was cooled down and re-analyzed. Its repeated dilatometric path in Fig. 2a inset reveals a thermal expansion behavior similar to the green body but with an apparent absence of the slope change associated with the basalt T_g, thus pointing out that substantial crystallization occurs during the sintering process.

Based on the dilatometric results, we selected three firing temperatures (1080, 1120, 1160 °C) for the conventional sintering (1 h) of the MGS-1 simulant. The specimens sintered at 1080 and 1120 °C had bulk densities of around 2.09 and 2.18 g/cm^3 respectively, resulting in limited densification. As expected, the samples produced at 1160 °C for 1 h were the densest, reaching a bulk density value of 2.39 g/cm^3. As such, the sintering evolution of the MGS-1 simulant was further investigated utilizing different dwell times and compared with FF (Fig. 3). Note that the heating time for the sample can be estimated in a matter of a few seconds. In previous work on FF of YSZ with similar sample thickness, the heating time was to equilibrate the temperature of about 7 s (Biesuz et al., 2024). This corresponds to a heating rate in the order of 10^2 °C/min.

It is worth noting that samples sintered by both methods did not exhibit any visible cracks, which could have been caused by thermal shock or other potential reasons. While the samples FFed for 1 min were not properly densified (ρ: 2.1 g/cm^3), those processed using conventional sintering exhibited a density of 2.24 g/cm^3. The conventionally sintered samples still had a higher density than FFed, when considering a firing time of 5 min. This is not surprising as conventional sintered specimens were heated at low rates thus being exposed to elevated temperatures for longer periods. On the other hand, when the sintering

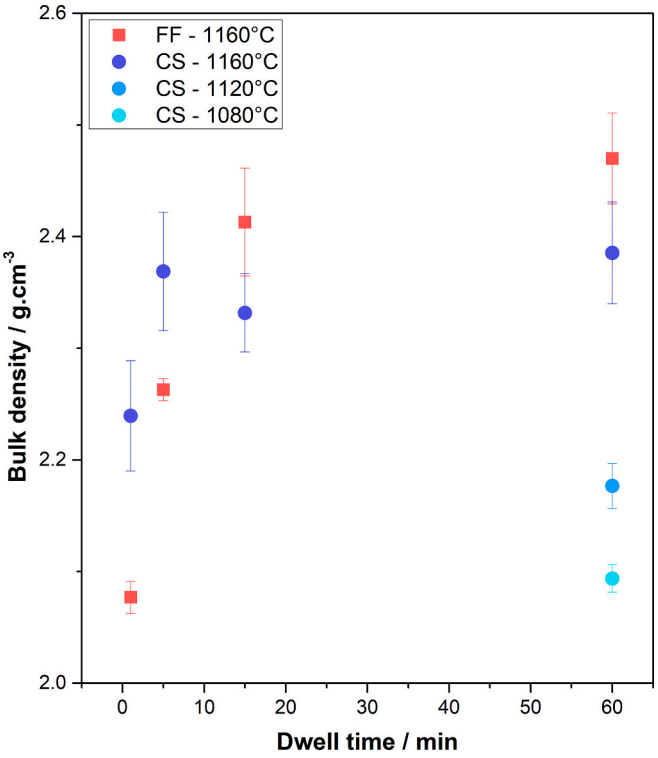

Fig. 3. The bulk density values of MGS-1 regolith compacts produced via conventional sintering and fast-firing process.

isotherm is longer than 15 min, it is evident that the densities of the samples produced by fast firing surpass those of conventional sintering. We can observe that most of the sintering takes place in the first 15 min, with only a slight enhancement in density for dwell time. These results confirm, in agreement with the dilatometric data, that rapid heating can facilitate the consolidation of the MGS-1 simulant and provide a valuable tool for ISRU.

Fig. 4 reports SEM micrographs of fast-fired and conventional sintered samples at 1160 °C for varying dwell times ranging from 1 to 60 min. The samples fabricated by both processes exhibited a heterogeneous microstructure similar to common traditional ceramic components. In samples produced within 1 min, only a weak bonding between particles takes place. Specifically, the samples FFed for 1 min possess porous microstructure. Substantial microstructural evolution can be detected after 5 min of dwell time. Considering the abundant presence of basalt glass and its T_g at around 910 °C, we can infer that it should contribute significantly to the densification process. As the dwell time progresses to 15 and 60 min, the samples get denser, and the porosity is reduced and partially converted from open (interconnected) to closed pores. The pore shape is rounded, suggesting their evolution within a possibly isotropic vitrified matrix, similar to traditional ceramics.

We can observe that the pore size in FF does not seem smaller than what is achieved by conventional sintering, so the origin of the enhanced densification by high heating rate must not lay on a mere microstructural refinement (generally observed in crystalline ceramics) leading to the larger capillarity stresses. This marks a clear distinction between the fast-firing behavior of the Martian regolith and crystalline ceramics, which lay on different physical phenomena. Besides, as expected, SEM micrographs reveal the presence of a considerable amount of Fe (white grains due to the SEM *Z*-contrast) in all samples.

Fig. 5**(a,b)** reports the X-ray diffraction patterns of the MGS-1 simulant powder, conventional sintered, and fast-fired specimens. All samples formed via conventional sintering and FF exhibited similar patterns with a high number of diffraction peaks that match those detected in the MGS-1 simulant powder but with different proportions between the main crystalline constituents. The main crystallographic phases detected by diffraction are plagioclase, $Ca_{0.88}Na_{0.12}Al_{1.77}Si_{2.23}O_8$ (ICDD # 00-052-1344); pyroxene $(Ca_{0.043}Mg_{1.155}Fe_{0.802})Si_2O_6$ (ICDD # 01-086-0163); forsterite $Mg_{1.8}Fe_{0.2}SiO_4$ (ICDD # 07-0075); hematite Fe_2O_3 (ICDD # 89-0597); and magnetite Fe_3O_4 (ICDD # 089-3854) (Karl

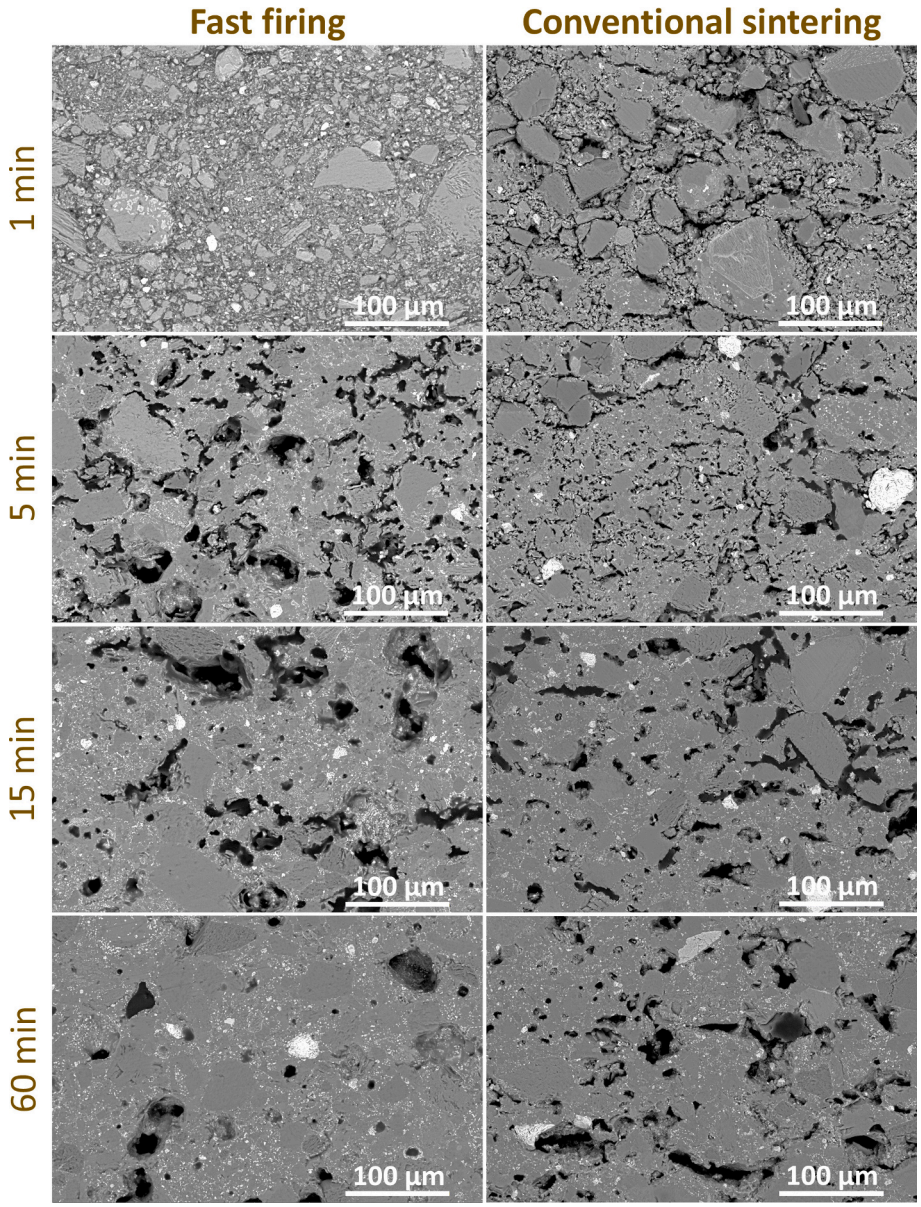

Fig. 4. Backscattered images obtained from polished MGS-1 specimens sintered by fast firing and conventionally using different holding times from 1 to 60 min.

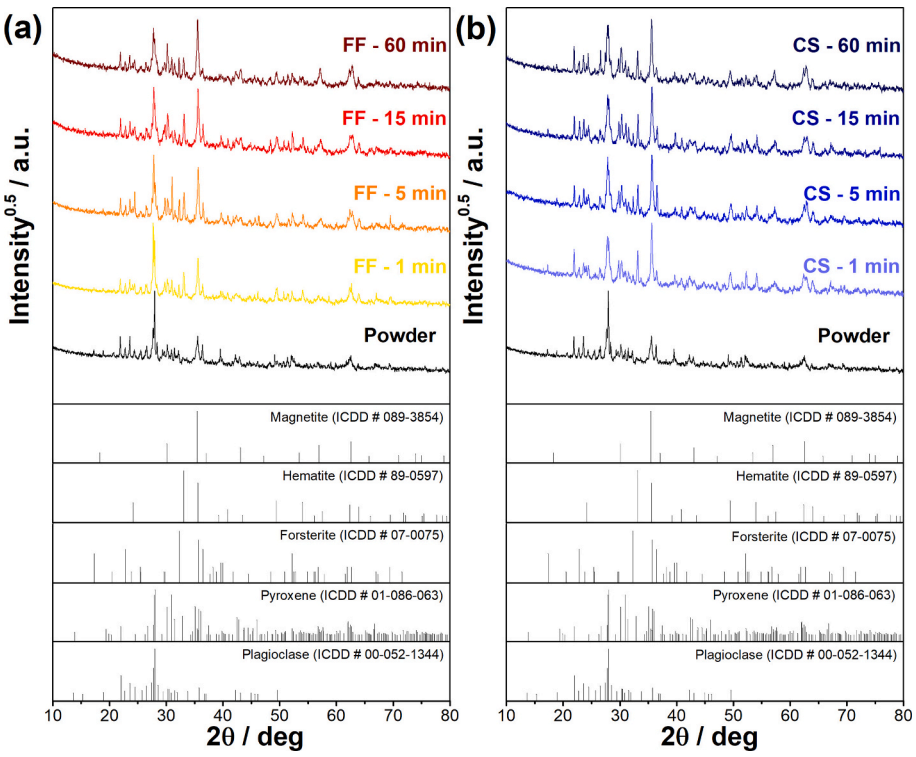

Fig. 5. X-ray diffraction patterns of **(a)** fast-fired samples at 1160 °C, **(b)** conventional sintered samples at 1160 °C with MGS-1 powder (as is, milled).

et al., 2020a; Pajares et al., 2024). It should be noted that when samples are conventionally sintered, the peak at 35.5° is the highest even after just 1 min of sintering, whereas it was only a secondary peak in the starting powder. In contrast, during FF the peak at 35.5° becomes dominant only after 15 min of dwell time and acquires an intensity similar to conventional sintering only after 1 h. Such a peak is related to the formation of iron oxides like hematite and magnetite. These can originate from the decomposition of Siderite (Fe-carbonate) and ferrihydrite in MGS-1 (Kądziołka-Gaweł et al., 2023). However, we can point out that these two phases account for only about 5 wt% of the regolith mass; therefore, they cannot explain the formation of such a strong diffraction feature alone. Hence, we can infer that the basalt glass partially crystallizes during the thermal treatment leading to the formation of iron oxide crystals. The crystallization of the basalt is fully consistent with the dilatometry in Fig. 2(a), which shows the disappearance of the basalt T_g after sintering.

Iron may exist in silicate glass in two forms, thus influencing the viscosity. Ferrous iron (Fe^{2+}) serves as a network modifier, thereby reducing the viscosity of the glass. In contrast, ferric iron (Fe^{3+}) acts as a network former (Kleest and Webb, 2022; Le Losq et al., 2021). We can observe that after 15 min of FF, the sample is definitively denser than after 1 min of conventional sintering, but the peak at 35.5° is not fully developed, as is the case with the conventionally sintered counterpart. This suggests a difference in the crystallization/sintering kinetics at different heating rates, where an evident retardation of crystallization phenomena is associated with rapid heating (in other words, the activation energy for sintering must be higher than that for the crystallization process). Hence, iron is still present in the glass structure at the firing temperature during FF, likely lowering the melt viscosity and enhancing sintering. On the other hand, during conventional heating, the glass in the simulant already largely crystalizes while heating with the formation of iron oxides, resulting in increased viscosity and a lower amount of glass. Such a result agrees well with previous reports on the sintering behavior of other silicate glass systems. For instance, Panda et al. showed that densification was significantly enhanced by increasing the heating rate in calcium aluminum-silicate glasses due to delayed crystallization (Panda et al., 1989). Therefore, fast firing enables higher densification of the simulant by altering crystallization, viscosity, and densification kinetics compared to conventional sintering.

The flexural strength data of the fast-fired and conventional sintered specimens at 1160 °C are given in Fig. 6 as a function of the firing time. Indeed, the strength obtained by both processes increases with

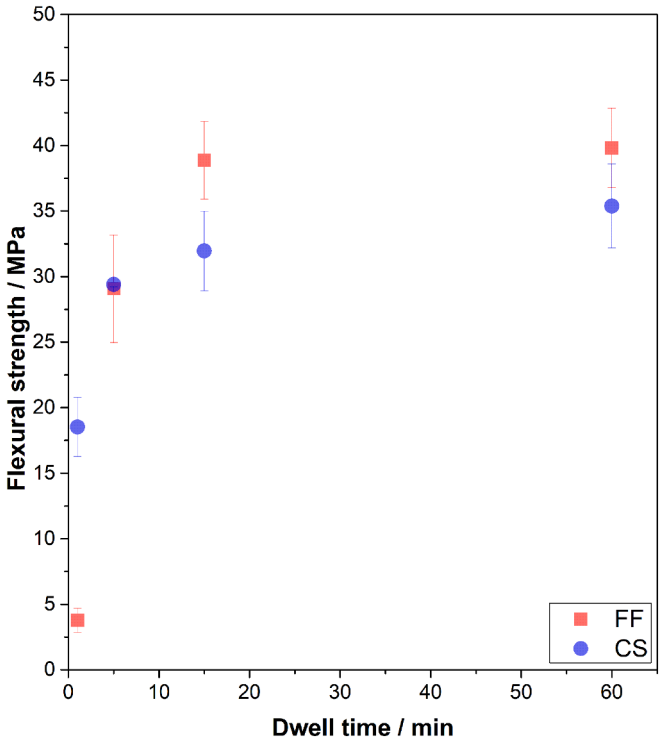

Fig. 6. Flexural strength values of fast-fired and conventional sintered MGS-1 regolith compacts produced at 1160 °C at different dwell times.

increasing dwell time. The FFed bodies are generally stronger than conventional sintered ones except for a dwell time of 1 min, thus mimicking the density evolution in Fig. 3. The FFed samples possess a flexural strength exceeding 35 MPa starting from the 15 min with only modest changes for longer dwell times. The evolution of mechanical strength can be attributed to different porosity volumes and morphologies, which are known to affect the stress concentration in the ceramic body (Romero and Pérez, 2015). Typical non-technical ceramics such as ceramic tiles, engineering brick, facing brick, and terracotta exhibit flexural strength of up to ~ 25 MPa, such values can be easily reached by the regolith simulant with a 15 min treatment by fast firing.

Fig. 7 reports a comparison of different ISRU approaches. The flexural strength utilizing different Mars regolith simulants (JSC-Mars-1A and MGS-1) is plotted against the amount of additives needed for shaping and processing the simulant. Most ISRU processes have reported a relatively low flexural strength when a large fraction of additives (e.g., water (Karl et al., 2020b; Morris et al., 2016), dispersant (Karl et al., 2020b), various binders, and solutions (Alexiadis et al., 2017; Buchner et al., 2018; Hedayati and Stulova, 2023; Sen et al., 2010; Shiwei et al., 2020; Tute and Goulas, 2024; Wan et al., 2016)) are used. Besides, some 3D printed simulants showed high strength values (up to 58 MPa (Karl et al., 2020b)), and such approaches require large amounts of additives that cannot be easily moved in extra-terrestrial environments. On the other hand, Chow et al. developed a specific type of dry consolidation involving high pressures (up to 800 MPa). This was applied on a different regolith simulant (JSC-Mars-1A), resulting in a flexural strength of 10–50 MPa (Chow et al., 2017). It is also worth noting that no transportation of additive material or material synthesis, i.e., binder, would be necessitated to produce sintered ceramics in this study. To evaluate the applicability of diverse ISRU material systems on Mars, their prior utilization on Earth is crucial, considering proper material systems with enough material availability, straightforward processing, and favorable properties over alternative options (Karl et al., 2020b). Besides, considering the widespread industrial utilization of fast firing, it could emerge as a promising candidate ISRU process, compared to the other methods, thereby stepping ahead in its applicability.

Despite various ISRU studies being developed, many have been commonly conducted under Earth's atmospheric conditions (Farries et al., 2021). It should be noted that there have been many reports on the influences of the sintering atmosphere on densification and properties of the technical ceramics (Kang, 2020). Some experiments have utilized different inert atmospheres (Dou et al., 2019), simulated the Martian atmosphere (Karl et al., 2020b), or have been carried out under vacuum conditions (Song et al., 2019) during the sintering processes of regoliths. In these studies, the obtained properties were usually superior compared to the samples produced in air (Han et al., 2022; Meurisse et al., 2017; Song et al., 2019). Consequently, atmosphere-controlled fast-firing systems (e.g., under vacuum (Mostaghaci and Brook, 1986)), could potentially play a significant role in future endeavors.

4. Conclusions

MGS-1 simulants without any additive were sintered by fast-firing as a different ISRU approach. The regolith compacts were densified at 1160 °C for varying dwell times ranging from 1 min to 1 h by comparing with conventional sintering method for the same conditions. If the dwell time at the firing temperature was longer than 15 min dwell, the specimens produced via fast-firing are denser and possess enhanced flexural strength values (>35 MPa) compared to the conventionally sintered materials. This is attributed to a heating rate-induced change in the densification/crystallization kinetics of the basalt glass in the simulant, where high heating rate promotes densification over crystallization. Fast-firing technique could be a promising approach in terms of ISRU.

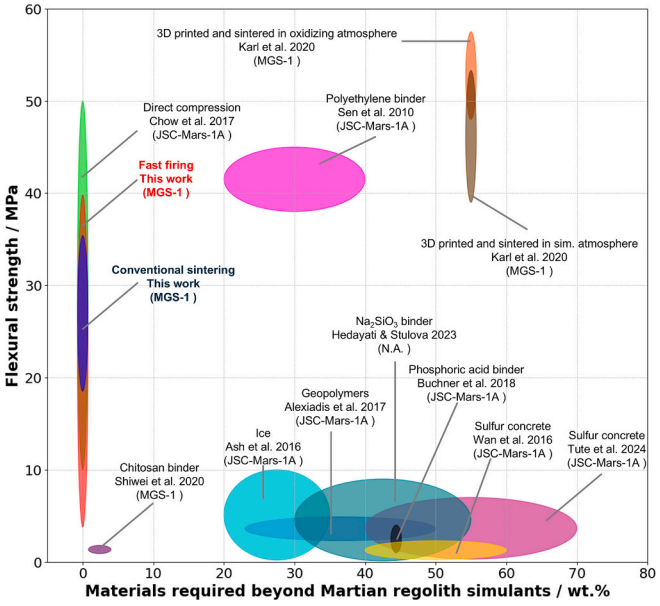

Fig. 7. Comparison of flexural strength values over additional materials required beyond Martian regolith simulants for ISRU approaches on Mars.

CRediT authorship contribution statement

Levent Karacasulu: Writing – original draft, Visualization, Methodology, Investigation, Data curation, Conceptualization. **Alessandro Tomasini:** Writing – original draft, Investigation, Data curation. **Cekdar Vakifahmetoglu:** Writing – review & editing, Supervision, Resources. **Mattia Biesuz:** Writing – review & editing, Supervision, Resources, Investigation, Conceptualization.

Declaration of competing interest

The authors declare that they have no known competing financial interests or personal relationships that could have appeared to influence the work reported in this paper.

Acknowledgments

Levent Karacasulu acknowledges the support of TUBITAK (The Scientific and Technological Research Council of Türkiye) within 2214-A - International Research Fellowship Programme for PhD students. CVA recognizes the İzmir Institute of Technology, the Center for Materials Research for characterizations.

Data availability

Data will be made available on request.

References

Alexiadis, A., Alberini, F., Meyer, M.E., 2017. Geopolymers from lunar and Martian soil simulants. Adv. Space Res. 59, 490–495. https://doi.org/10.1016/j.asr.2016.10.003.

Allen, C.C., Jager, K.M., Morris, R.V., Lindstrom, D.J., Lindstrom, M.M., Lockwood, J.P., 1998a. JSC Mars-1: a Martian soil simulant. In: Space, vol. 98, pp. 469–476. https://doi.org/10.1061/40339(206)54.

Allen, C.C., Jager, K.M., Morris, R.V., Lindstrom, D.J., Lindtsrom, M.M., Lockwood, J.P., 1998b. Martian soil simulant available for scientific, educational study. EOS Trans. Am. Geophys. Union 79, 405–409. https://doi.org/10.1029/98EO00309.

Altun, A.A., Ertl, F., Marechal, M., Makaya, A., Sgambati, A., Schwentenwein, M., 2021. Additive manufacturing of lunar regolith structures. Open Ceram. 5, 100058. https://doi.org/10.1016/j.oceram.2021.100058.

Biesuz, M., De Bona, E., Manière, C., 2024. Fast firing of 3 Mol% yttria-stabilized zirconia: on the effect of heating rate on sintering. J. Am. Ceram. Soc. 107, 6596–6606. https://doi.org/10.1111/jace.19989.

Bish, D.L., et al., 2013. X-ray diffraction Results from Mars science laboratory: mineralogy of Rocknest at Gale crater. Science 1979, 341. https://doi.org/10.1126/science.1238932.
Blacic, J.D., 1985. Mechanical properties of lunar materials under anhydrous, hard vacuum conditions: applications of lunar glass structural components. In: Lunar Bases and Space Activities of the 21st Century, p. 487.
Bordia, R.K., Kang, S.-J.L., Olevsky, E.A., 2017. Current understanding and future research directions at the onset of the next century of sintering science and technology. J. Am. Ceram. Soc. 100, 2314–2352. https://doi.org/10.1111/jace.14919.
Buchner, C., Pawelke, R.H., Schlauf, T., Reissner, A., Makaya, A., 2018. A new planetary structure fabrication process using phosphoric acid. Acta Astronaut. 143, 272–284. https://doi.org/10.1016/j.actaastro.2017.11.045.
Cannon, K.M., Britt, D.T., Smith, T.M., Fritsche, R.F., Batcheldor, D., 2019. Mars global simulant MGS-1: a Rocknest-based open standard for basaltic martian regolith simulants. Icarus 317, 470–478. https://doi.org/10.1016/j.icarus.2018.08.019.
Chow, B.J., Chen, T., Zhong, Y., Qiao, Y., 2017. Direct formation of structural components using a Martian soil simulant. Sci. Rep. 7, 1151. https://doi.org/10.1038/s41598-017-01157-w.
Clark, J.V., Archer, P.D., Gruener, J.E., Ming, D.W., Tu, V.M., Niles, P.B., Mertzman, S.A., 2020. JSC-Rocknest: a large-scale Mojave Mars simulant (MMS) based soil simulant for in-situ resource utilization water-extraction studies. Icarus 351, 113936. https://doi.org/10.1016/j.icarus.2020.113936.
Corrias, G., Licheri, R., Orrù, R., Cao, G., 2012. Self-propagating high-temperature reactions for the fabrication of lunar and Martian physical assets. Acta Astronaut. 70, 69–76. https://doi.org/10.1016/j.actaastro.2011.07.022.
Dalton, C., Hohmann, E., 1972. Conceptual Design of a Lunar Colony. NASA/ASEE Systems Design Institute.
Dou, R., Tang, W.Z., Wang, L., Li, S., Duan, W.Y., Liu, M., Zhang, Y.B., Wang, G., 2019. Sintering of lunar regolith structures fabricated via digital light processing. Ceram. Int. 45, 17210–17215. https://doi.org/10.1016/j.ceramint.2019.05.276.
Farries, K.W., Visintin, P., Smith, S.T., van Eyk, P., 2021. Sintered or melted regolith for lunar construction: state-of-the-art review and future research directions. Constr. Build. Mater. 296, 123627. https://doi.org/10.1016/j.conbuildmat.2021.123627.
Farries, K.W., Visintin, P., Smith, S.T., 2022. Direct laser sintering for lunar dust control: an experimental study of the effect of simulant mineralogy and process parameters on product strength and scalability. Constr. Build. Mater. 354, 129191. https://doi.org/10.1016/j.conbuildmat.2022.129191.
Fateri, M., Gebhardt, A., 2015. Process parameters development of selective laser melting of lunar regolith for on-site manufacturing applications. Int. J. Appl. Ceram. Technol. 12, 46–52. https://doi.org/10.1111/ijac.12326.
Ginés-Palomares, J.-C., Fateri, M., Kalhöfer, E., Schubert, T., Meyer, L., Kolsch, N., Brandić Lipińska, M., Davenport, R., Imhof, B., Waclavicek, R., Sperl, M., Makaya, A., Günster, J., 2023. Laser melting manufacturing of large elements of lunar regolith simulant for paving on the moon. Sci. Rep. 13, 15593. https://doi.org/10.1038/s41598-023-42008-1.
Gupta, N., Dawara, V., Kumar, A., Viswanathan, K., 2024. Synthetic space bricks from lunar and Martian regolith via sintering. Adv. Space Res. https://doi.org/10.1016/j.asr.2024.06.045.
Han, W., Ding, L., Cai, L., Zhu, J., Luo, H., Tang, T., 2022. Sintering of HUST-1 lunar regolith simulant. Constr. Build. Mater. 324, 126655. https://doi.org/10.1016/j.conbuildmat.2022.126655.
Harmer, M.P., Brook, R.J., 1981. Fast firing-microstructural benefits. Trans. J. Br. Ceram. Soc. 80, 147–148.
Hedayati, R., Stulova, V., 2023. 3D printing of habitats on Mars: effects of low temperature and pressure. Materials 16, 5175. https://doi.org/10.3390/ma16145175.
Hintze, P.E., Stephanie, Q., 2013. Building a lunar or Martian launch pad with in situ materials: recent laboratory and field studies. J. Aerosp. Eng. 26, 134–142. https://doi.org/10.1061/(ASCE)AS.1943-5525.0000205.
Hotza, D., García, D.E., Castro, R.H.R., 2015. Obtaining highly dense YSZ nanoceramics by pressureless, unassisted sintering. Int. Mater. Rev. 60, 353–375. https://doi.org/10.1179/1743280415Y.0000000005.
Kądziołka-Gaweł, M., Nowak, J., Szubka, M., Klimontko, J., Wojtyniak, M., 2023. Thermal decomposition of siderite and characterization of the decomposition products under O_2 and CO_2 atmospheres. Minerals 13, 1066. https://doi.org/10.3390/min13081066.
Kang, S.-J.L., 2020. What we should consider for full densification when sintering. Materials 13, 3578. https://doi.org/10.3390/ma13163578.
Karacasulu, L., Karl, D., Gurlo, A., Vakifahmetoglu, C., 2023. Cold sintering as a promising ISRU technique: a case study of Mars regolith simulant. Icarus 389, 115270. https://doi.org/10.1016/j.icarus.2022.115270.
Karacasulu, L., Karakaya, M., Adem, U., Sglavo, V.M., Biesuz, M., Vakifahmetoglu, C., 2024. Fast-firing of potassium sodium niobate (KNN). Open Ceram. 17, 100541. https://doi.org/10.1016/j.oceram.2024.100541.
Karl, D., Kamutzki, F., Zocca, A., Goerke, O., Guenster, J., Gurlo, A., 2018. Towards the colonization of Mars by in-situ resource utilization: slip cast ceramics from Martian soil simulant. PLoS One 13, e0204025. https://doi.org/10.1371/journal.pone.0204025.
Karl, D., Duminy, T., Lima, P., Kamutzki, F., Gili, A., Zocca, A., Günster, J., Gurlo, A., 2020a. Clay in situ resource utilization with Mars global simulant slurries for additive manufacturing and traditional shaping of unfired green bodies. Acta Astronaut. 174, 241–253. https://doi.org/10.1016/j.actaastro.2020.04.064.
Karl, D., Kamutzki, F., Lima, P., Gili, A., Duminy, T., Zocca, A., Günster, J., Gurlo, A., 2020b. Sintering of ceramics for clay in situ resource utilization on Mars. Open Ceram. 3, 100008. https://doi.org/10.1016/j.oceram.2020.100008.
Karl, D., Cannon, K.M., Gurlo, A., 2022. Review of space resources processing for Mars missions: Martian simulants, regolith bonding concepts and additive manufacturing. Open Ceram. 9, 100216. https://doi.org/10.1016/j.oceram.2021.100216.
Kim, D.-H., Kim, C.H., 1993. Effect of heating rate on pore shrinkage in Yttria-doped zirconia. J. Am. Ceram. Soc. 76, 1877–1878. https://doi.org/10.1111/j.1151-2916.1993.tb06665.x.
Kim, Y.-J., Ryu, B.H., Jin, H., Lee, J., Shin, H.-S., 2021. Microstructural, mechanical, and thermal properties of microwave-sintered KLS-1 lunar regolith simulant. Ceram. Int. 47, 26891–26897. https://doi.org/10.1016/j.ceramint.2021.06.098.
Kleest, C., Webb, S.L., 2022. Influence of Fe^{2+}/Fe_{tot} on the viscosity of melts from the Colli Albani Volcanic District (Italy) – foidite to phonolite. J. Volcanol. Geotherm. Res. 431, 107649. https://doi.org/10.1016/j.jvolgeores.2022.107649.
Krishna Balla, V., Roberson, L.B., O'Connor, G.W., Trigwell, S., Bose, S., Bandyopadhyay, A., 2012. First demonstration on direct laser fabrication of lunar regolith parts. Rapid Prototyp. J. 18, 451–457. https://doi.org/10.1108/13552541211271992.
Le Losq, C., Cicconi, M.R., Neuville, D.R., 2021. Iron in silicate glasses and melts. In: Magma Redox Geochemistry, Geophysical Monograph Series, pp. 233–253. https://doi.org/10.1002/9781119473206.ch12.
Leriche, A., Cambier, F., Hampshire, S., 2017. Sintering of ceramics. In: Reference Module in Materials Science and Materials Engineering. Elsevier. https://doi.org/10.1016/B978-0-12-803581-8.10288-7.
Licheri, R., Orrù, R., Sani, E., Dell'Oro, A., Cao, G., 2022. Spark plasma sintering and optical characterization of lunar regolith simulant. Acta Astronaut. 201, 164–171. https://doi.org/10.1016/j.actaastro.2022.09.016.
Lim, S., Bowen, J., Degli-Alessandrini, G., Anand, M., Cowley, A., Levin Prabhu, V., 2021. Investigating the microwave heating behaviour of lunar soil simulant JSC-1A at different input powers. Sci. Rep. 11, 2133. https://doi.org/10.1038/s41598-021-81691-w.
Long-Fox, J.M., Britt, D.T., 2023. Characterization of planetary regolith simulants for the research and development of space resource technologies. Front. Space Technol. 4. https://doi.org/10.3389/frspt.2023.1255535.
Martikainen, J., Muñoz, O., Jardiel, T., Martín, J.C.G., Peiteado, M., Willame, Y., Penttilä, A., Muinonen, K., Wurm, G., Becker, T., 2023. Optical constants of Martian dust analogs at UV–visible–near-infrared wavelengths. Astrophys. J. Suppl. Ser. 268, 47. https://doi.org/10.3847/1538-4365/acf0be.
Meek, T.T., Vaniman, D.T., Blake, R.D., Godbole, M.J., 1987. Sintering of lunar soil simulants using 2.45 GHz microwave radiation. In: Lunar and Planetary Science Conference 18, 635–636.
Meurisse, A., Beltzung, J.C., Kolbe, M., Cowley, A., Sperl, M., 2017. Influence of mineral composition on sintering lunar regolith. J. Aerosp. Eng. 30, 04017014. https://doi.org/10.1061/(ASCE)AS.1943-5525.0000721.
Meurisse, A., Makaya, A., Willsch, C., Sperl, M., 2018. Solar 3D printing of lunar regolith. Acta Astronaut. 152, 800–810. https://doi.org/10.1016/j.actaastro.2018.06.063.
Mills, J.N., Katzarova, M., Wagner, N.J., 2022. Comparison of lunar and Martian regolith simulant-based geopolymer cements formed by alkali-activation for in-situ resource utilization. Adv. Space Res. 69, 761–777. https://doi.org/10.1016/j.asr.2021.10.045.
Montes, C., Broussard, K., Gongre, M., Simicevic, N., Mejia, J., Tham, J., Allouche, E., Davis, G., 2015. Evaluation of lunar regolith geopolymer binder as a radioactive shielding material for space exploration applications. Adv. Space Res. 56, 1212–1221. https://doi.org/10.1016/j.asr.2015.05.044.
Morris, M., Ciardullo, C., Lents, K., Montes, J., Rudakevych, O., Sono, M., Sono, Y., Yashar, M., 2016. Mars ice house: using the physics of phase change in 3D printing a habitat with H_2O. In: AIAA SPACE 2016, AIAA SPACE Forum. American Institute of Aeronautics and Astronautics. https://doi.org/10.2514/6.2016-5528.
Moses, R.W., Bushnell, D.M., 2016. Frontier In-Situ Resource Utilization for Enabling Sustained Human Presence on Mars. National Aeronautics and Space Administration, Langley Research Center, pp. NF1676L–20756.
Mostaghaci, H., Brook, R.J., 1986. Microstructure development and dielectric properties of fast-fired $BaTiO_3$ ceramics. J. Mater. Sci. 21, 3575–3580. https://doi.org/10.1007/BF00553803.
Naser, M.Z., 2019. Extraterrestrial construction materials. Prog. Mater. Sci. 105, 100577. https://doi.org/10.1016/j.pmatsci.2019.100577.
Pajares, A., Guardia, P., Galvita, V., Conti, M., Lefevere, J., Michielsen, B., 2024. CO_2 conversion over Martian and lunar regolith simulants for extraterrestrial applications. J. CO2 Utiliz. 81, 102729. https://doi.org/10.1016/j.jcou.2024.102729.
Panda, P.C., Mobley, W.M., Raj, R., 1989. Effect of the heating rate on the relative rates of sintering and crystallization in glass. J. Am. Ceram. Soc. 72, 2361–2364. https://doi.org/10.1111/j.1151-2916.1989.tb06090.x.
Roberts, A.D., Whittall, D.R., Breitling, R., Takano, E., Blaker, J.J., Hay, S., Scrutton, N. S., 2021. Blood, sweat, and tears: extraterrestrial regolith biocomposites with in vivo binders. Mater Today Bio 12, 100136. https://doi.org/10.1016/j.mtbio.2021.100136.
Romero, M., Pérez, J.M., 2015. Relation between the microstructure and technological properties of porcelain stoneware. A review. Mater. Constr. 65 (320), e065. https://doi.org/10.3989/mc.2015.05915.
Rousek, T., Eriksson, K., Doule, O., 2012. SinterHab. Acta Astronaut. 74, 98–111. https://doi.org/10.1016/j.actaastro.2011.10.009.
Sen, S., Carranza, S., Pillay, S., 2010. Multifunctional Martian habitat composite material synthesized from in situ resources. Adv. Space Res. 46, 582–592. https://doi.org/10.1016/j.asr.2010.04.009.
Shetty, D.K, Rosenfield, A.R., McGuire, P., Bansal, G.K., Duckworth, W.H., 1980. Biaxial flexure tests for ceramics. Am. Ceram. Soc. Bull. 59, 12.

Shiwei, N., Dritsas, S., Fernandez, J.G., 2020. Martian biolith: a bioinspired regolith composite for closed-loop extraterrestrial manufacturing. PLoS One 15, e0238606. https://doi.org/10.1371/journal.pone.0238606.

Simonds, C.H., 1973. Sintering and Hot Pressing of Fra Mauro Composition Glass and the Lithification of Lunar Breccias. Am. J. Sci. 273. https://doi.org/10.2475/ajs.273.5.428.

Song, L., Xu, J., Fan, S., Tang, H., Li, X., Liu, J., Duan, X., 2019. Vacuum sintered lunar regolith simulant: pore-forming and thermal conductivity. Ceram. Int. 45, 3627–3633. https://doi.org/10.1016/j.ceramint.2018.11.023.

Taylor, L.A., Meek, T.T., 2005. Microwave sintering of lunar soil: properties, theory, and practice. J. Aerosp. Eng. 18, 188–196. https://doi.org/10.1061/(ASCE)0893-1321(2005)18:3(188).

Tute, R.M., Goulas, A., 2024. Mechanical behaviour of Sulphur-based Martian regolith concrete processed under CO_2-rich conditions. Icarus 417, 116134. https://doi.org/10.1016/j.icarus.2024.116134.

Wan, L., Wendner, R., Cusatis, G., 2016. A novel material for in situ construction on Mars: experiments and numerical simulations. Constr. Build. Mater. 120, 222–231. https://doi.org/10.1016/j.conbuildmat.2016.05.046.

Warren, P., Raju, N., Ebrahimi, H., Krsmanovic, M., Raghavan, S., Kapat, J., Ghosh, R., 2022. Effect of sintering temperature on microstructure and mechanical properties of molded Martian and lunar regolith. Ceram. Int. 48, 35825–35833. https://doi.org/10.1016/j.ceramint.2022.07.329.

Zocca, A., Fateri, M., Al-Sabbagh, D., Günster, J., 2020. Investigation of the sintering and melting of JSC-2A lunar regolith simulant. Ceram. Int. 46, 14097–14104. https://doi.org/10.1016/j.ceramint.2020.02.212.